THE JOURNAL OF PHYSICAL CHEMISTRY B

Article

pubs.acs.org/JPCB

Free Energetics and the Role of Water in the Permeation of Methyl Guanidinium across the Bilayer–Water Interface: Insights from Molecular Dynamics Simulations Using Charge Equilibration Potentials

Shuching Ou,[†] Timothy R. Lucas,[†] Yang Zhong,[†,§] Brad A. Bauer,[‡] Yuan Hu,[†] and Sandeep Patel*[,†]

[†]Department of Chemistry and Biochemistry, University of Delaware, Newark, Delaware 19716, United States

[‡]Department of Physical and Biological Sciences, The College of Saint Rose, Albany, New York 12203, United States

[§]Genomics Institute of the Novartis Research Foundation, 10675 John J. Hopkins Drive, San Diego, California 92121, United States

Supporting Information

ABSTRACT: Combining umbrella sampling molecular dynamics (MD) simulations, the weighted histogram analysis method (WHAM) for unbiasing probabilities, and polarizable charge equilibration force fields, we compute the potential of mean force for the reversible transfer of methyl guanidinium from bulk solution to the center of a model DPPC bilayer. A 5 kcal/mol minimum in the potential of mean force profile for membrane permeation suggests that the analogue will preferentially reside in the headgroup region of the lipid, qualitatively in agreement with previously published results. We find the potential of mean force for permeation to be approximately 28 kcal/mol (relative to the minimum in the headgroups), within the range of values reported for similar types of simulations using fixed-charge force fields. From analysis of the lipid structure, we find that the lipid deformation leads to a substantial destabilizing contribution to the free energy of the methyl guanidinium as it resides in the bilayer center, though this deformation allows more efficient stabilization by water defects and transient pores. Water in the bilayer core stabilizes the charged residue. The role of water in stabilizing or destabilizing the solute as it crosses the bilayer depends on bulk electrolyte concentration. In 1 M KCl solution, the water contribution to the potential of mean force is stabilizing over the entire range of the permeation coordinate, with the sole destabilizing force originating from the anionic species in solution. Conversely, methyl guanidinium experiences net destabilization from water in the absence of electrolyte. The difference in solvent contributions to permeation free energy is traced to a local effect arising from differences in water density in the bilayer–water solution interface, thus leading to starkly opposite net forces on the permeant. The origin of the local water density differential rests with the penetration of hydrated chloride anions into the solution–bilayer interface. Finally, water permeation into the bilayer is required for the deformation of individual lipid molecules and permeation of ions into the membrane. From simulations where water is first excluded from the bilayer center where methyl guanidinium is restrained and then, after equilibration, allowed to enter the bilayer, we find that in the absence of any water defects/permeation into the bilayer, the lipid headgroups do not follow the methyl guanidinium. Only when water enters the bilayer do we see deformation of individual lipid molecules to associate with the amino acid analogue at bilayer center.

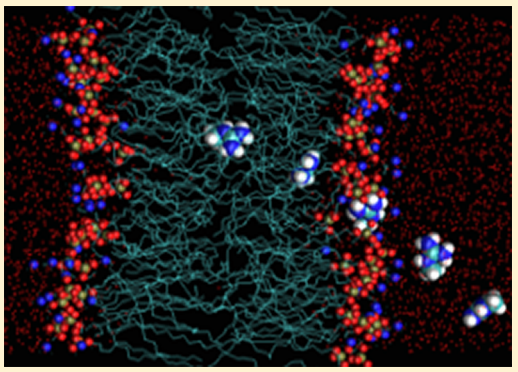

I. INTRODUCTION

Recent years have witnessed great interest in the understanding of the molecular origins of the presence of charged and polar amino acid residues in ostensibly hydrophobic lipid bilayer environments.[1−13] The motivation for such a microscopic understanding stems from the broad range of biophysical processes predicated on the interactions between such protein residues and hydrophobic lipid chains. These processes range from voltage gating in select ion channels,[14−16] permeation of cationic residue enriched cell-penetrating peptides for transporting cargo across the cellular membrane,[17−23] and the action of antimicrobial peptides upon interaction with native cellular membranes. Understanding of these protein–lipid interactions has sought recourse in hydrophobicity scales quantifying relative partitioning propensities of different amino acid side chains from aqueous to bilayer-like environments.[24] Elaborating upon ideas of partitioning of functional chemical groups between hydrophilic and hydrophobic environments, recent work has broadened the palette of hydrophobicity scales attempting to address the relative free energetics of

Received: July 22, 2012
Revised: February 8, 2013
Published: February 14, 2013

partitioning; this has been possible due to novel experiments on well-characterized integral-membrane protein systems[8] as well as elucidation of structural aspects of the machinery implicated in the synthesis and insertion of membrane proteins upon synthesis in the ribosome.[25] More recently, there appears to be a convergence of molecular modeling based predictions of relative free energetics of different amino acid side chains as part of a macromolecular assembly and experiment.[7] Further factors possibly contributing to interactions of charge and polar species in lipid bilayers include bilayer thickness, nonadditivity of interactions between nonbilayer components,[26,27] specificity of protein sequence to specific bilayer composition,[28−31] interactions of a particular amino side chain in the bilayer with lipid headgroups and water, and lipid deformation (coupled with the ease of deformability of the lipid).[10,18,32]

In conjunction with recent experimental advances in studying the relative stability of charged amino acid residues in bilayer environments (within several contexts including cell-penetrating peptides, the presence of charged voltage gating and sensing domains in potassium channels, and other biochemical transformations), there has been a steady push for developing novel molecular modeling methods for treating the heterogeneous environments presented by lipid bilayers of various compositions. In particular, nonadditive force fields are being pursued for modeling lipid bilayers. Though nonadditive force fields have been pursued for over two decades now, only recently have there been substantial, published studies documenting the application of such models to the study of biophysical problems of general interest.[33−46,46−54] Recently, we, along with others, have published results of the first applications of polarizable, nonadditive force fields for treating lipid bilayers in a fully atomistic molecular simulation. We have been developing a class of nonadditive, polarizable force fields based on the charge equilibration (CHEQ) or fluctuating charge (FQ) formalism. One of the first attempts to apply CHEQ-based force fields to lipid bilayers was by Shimizu and co-workers;[55] in their study, the authors explored the consequence of the extent of charge transfer in extended systems defining the nature of charge transfer effects and possible hyper-polarization in such models. The authors demonstrated the need for some approach to control the superlinear polarizability in applying charge equilibration models in a manner that does not constrain charge transfer in a systematic and physically meaningful way. Recently, Vacha et al.[56] applied a fully polarizable force field (lipid, water, and ions) to the study of monovalent ion interactions with phosphatidylcholine membranes and associated effects at the membrane−water interface. Furthermore, Harder et al.[45] examined the difference in the interfacial dipole potential between the pure liquid−vapor interface of water and that of a DPPC monolayer. The authors presented the case for polarization helping to accurately predict the potential difference between these two systems compared to existing nonpolarizable force fields. Over the last several years, our group has been involved in a substantial effort to develop nonadditive electrostatic models for lipid bilayers to be used in conjunction with molecular dynamics simulations. We have presented a systematic parametrization of a first-generation charge equilibration force field based on the DPPC lipid.[54,57] In this study, we continue further application of our models to explore the free energetics of an analogue of arginine, methyl guanidinium, in a model DPPC bilayer. This complements earlier studies using both polarizable and nonpolarizable force fields in conjunction with molecular dynamics simulations to study this canonical system. We do not claim that polarizable force fields are a panacea to all deficiencies of the current state of the art force fields; this study further explores applications of current polarizable force field technology to systems of biochemical interest.

In this work, we continue to explore the free energetics of charged species, in this case methyl guanidinium, permeating across a model lipid bilayer. We consider a model DPPC bilayer as the oft-used proxy for a physiological membrane. We consider pure water and 1 M KCl systems, the salt concentration being higher than physiological conditions to sufficiently sample configurations of the ions in the vicinity of the membrane−water interface. We further explore the nature of water and its ability to mediate deformations of the lipid bilayer in stabilizing a charged species at the center of this model bilayer. There has been much literature on the permeation of polar and charged solutes into lipid membranes with an accompanying hydration shell of water molecules.[12,13] We address the idea that this accompanying water also mediates the interactions between the lipid headgroups and permeating solute. We attempt to study this effect by performing molecular simulations where water is expelled from the core of the bilayer. We then proceed to remove this constraint to observe any deformations that accompany the permeation of water into the bilayer. Section II discusses general aspects of the charge equilibration force field and its implementation. Section IIC addresses the validation of the methyl guanidinium force field through the calculation of hydration enthalpies and comparison to previous literature data. Section IID discusses results of the potential of mean force (PMF) for methyl guanidinium permeation. Section III presents extended discussion of the results of hydration free energy calculations, the potential of mean force, decomposition of the potential of mean force into contributions from system components, an explanation of the differences of the PMFs computed in salt solution versus pure aqueous environments, and finally discussion of the role of water in potentially mediating membrane deformation. Section IV concludes with a summary and final thoughts.

II. METHODS

A. Charge Equilibration Force Fields. We next consider details of the charge equilibration (CHEQ) method and considerations in our specific implementation of this method. An additive (or *nonpolarizable*) formalism for force fields is based on the construct that all atomic partial charges are fixed throughout the course of the simulations. Alternatively, we can consider the variation of atomic partial charge using the CHEQ formalism.[46,58−67] The CHEQ formalism is based on Sanderson's idea of electronegativity equilibration[66,67] in which the chemical potential is equilibrated via the redistribution of charge density. In a classical sense, charge density is reduced to partial charges, Q_α, on each atomic site α. The charge-dependent energy for a system of M molecules containing N_i atoms per molecule is then expressed as

dx.doi.org/10.1021/jp400389z | J. Phys. Chem. B 2013, 117, 3578−3592

$$E_{\mathrm{CHEQ}}(\vec{R}, \vec{Q}) = \sum_{i=1}^{M}\sum_{\alpha=1}^{N}\chi_{i\alpha}Q_{i\alpha} + \frac{1}{2}\sum_{i=1}^{M}\sum_{j=1}^{M}\sum_{\alpha=1}^{N_i}\sum_{\beta=1}^{N_j}J_{i\alpha j\beta}Q_{i\alpha}Q_{j\beta} + \frac{1}{2}\sum_{i=1}^{MN}{}'\sum_{j=1}^{MN}{}'\frac{Q_iQ_j}{4\pi\varepsilon_0 r_{ij}} + \sum_{j=1}^{M}\lambda_j\left(\sum_{i=1}^{N}Q_{ji} - Q_j^{\mathrm{Total}}\right) \quad (1)$$

where the χ terms represent the atomic electronegativities which control the directionality of electron flow and J terms represent the atomic hardnesses which control the resistance to electron flow to or from the atom. Although these parameters are derived from the definitions of electron affinity and ionization potential, they are treated as empirical parameters for individual atom types. Heterogeneous hardness elements that describe the interaction between two different atom types are calculated using the combining rule[68] on the parametrized homogeneous hardness elements (J_{ii}°)

$$J_{ij}(R_{ij}, J_{ii}^{\circ}, J_{jj}^{\circ}) = \frac{\frac{1}{2}(J_{ii}^{\circ} + J_{jj}^{\circ})}{\sqrt{1.0 + \frac{1}{4}(J_{ii}^{\circ} + J_{jj}^{\circ})^2 R_{ij}^2}} \quad (2)$$

where R_{ij} is the distance between atoms i and j. This combination locally screens Coulombic interactions but provides the correct limiting behavior at atomic separations greater than approximately 2.5 Å. The standard Coulomb interaction between sites not involved in the dihedral, angle, or bonded interactions (denoted by primed summation) with each other is included as the third term in eq 1. The second term in eq 1 represents the local charge transfer interaction, which is usually restricted to within a molecule or an appropriate charge normalization unit. Currently, we do not consider intermolecular charge transfer, although approaches to incorporate this effect have recently been developed and applied to liquid water.[69] Charge is constrained via a Lagrange multiplier, λ, which is included for each molecule as indicated in the last term of eq 1. We remark that use of multiple charge normalization units can modulate molecular polarizability by limiting intramolecular charge transfer to physical distances. Such an approach controls previously observed superlinear polarizability scaling,[53,70,71] which also manifests as the polarization catastrophe (in point polarizable force fields),[53,72] while also developing a construct for piecing together small molecular entities into macromolecules. The molecular polarizability in the CHEQ formalism can be calculated as[53]

$$\alpha_{\gamma\beta} = \mathbf{R}_{\beta}^{T}\mathbf{J}'^{-1}\mathbf{R}_{\gamma} \quad (3)$$

where $\mathbf{J}'$ is the atomic hardness matrix augmented with the appropriate rows and columns to treat the charge conservation constraints. $\mathbf{R}_{\gamma}$ and $\mathbf{R}_{\beta}$ are the γ and β Cartesian coordinates of the atomic position vectors; these vectors are augmented to appropriately match the dimensions of the atomic hardness matrix. Representative values for the molecular polarizability for a wide variety of small molecule analogues of biomolecular functional groups are given in ref 58.

Charge degrees of freedom are propagated via an extended Lagrangian formulation, thus providing for electronegativity equilibration at each dynamics step. The system Lagrangian is

$$L = \sum_{i=1}^{M}\sum_{\alpha=1}^{N}\frac{1}{2}m_{i\alpha}\left(\frac{dr_{i\alpha}}{dt}\right)^2 + \sum_{i=1}^{M}\sum_{\alpha=1}^{N}\frac{1}{2}m_{Q,i\alpha}\left(\frac{dQ_{i\alpha}}{dt}\right)^2 - E(Q, r) - \sum_{i=1}^{M}\lambda_i\left(\left(\sum_{\alpha=1}^{N}Q_{i\alpha}\right) - Q_i^{\mathrm{total}}\right) \quad (4)$$

where the first two terms represent the nuclear and charge kinetic energies; the third term is the potential energy; and the fourth term is the molecular charge neutrality constraint enforced on each molecule i via a Lagrange multiplier λ_i. The fictitious charge dynamics are determined using a charge "mass" with units of (energy time^2/charge^2), which is analogous to the use of an adiabaticity parameter in fictitious wave function dynamics in Car–Parrinello (CP) type methods.[61,73] Charges are propagated based on the forces arising from differences between the average electronegativity of a molecule and the instantaneous electronegativity at an atomic site.

B. Simulation Setup. The membrane system consists of 72 DPPC lipid molecules, arranged in a bilayer (36 molecules per leaflet), solvated with an approximately 1 M potassium chloride solution composed of 3203 TIP4P-FQ water molecules,[61] 57 K^+, and 58 Cl^- ions and containing a single positively charged methyl guanidinium (mguanH^+) molecule. We performed molecular dynamics simulations using the CHEQ formalism in the constant particle, normal pressure, lateral surface area, and temperature (NP_AT) ensemble at a pressure of 1 atm, a temperature of 323 K, and an area per lipid of 63.0 Å^2, above the temperature of the liquid–gel phase transition[74] and within the experimental range for the area per lipid.[75] The pressure was maintained using the Langevin piston method[76] with a piston mass of 2025 amu in the z-direction, normal to the bilayer. The temperature of the simulation was controlled using the Nosé–Hoover method[76,77] with a thermal piston mass of 3000 kcal/mol·ps^2. Long-range electrostatics were accounted for by the particle mesh Ewald (PME) summation[78,79] with a 48 × 48 × 80 Å^3 fast Fourier transform (FFT) grid, fourth-order B-spline interpolation, and screening parameter κ = 0.32. Dynamics were propagated using the Leapfrog Verlet integrator[76] with a 0.5 fs time step.

The CHEQ lipid force field has been developed and validated based on NVT ensemble simulations of hydrated bilayer and monolayer systems.[50,54,57] In the current simulations we use an intermediate, revised version of the CHEQ lipid force field in which (1) the Lennard-Jones (LJ) nonbonded parameters between headgroup atoms were varied to facilitate surface tensionless MD simulations in constant NPT simulations and (2) selected dihedral parameters were adjusted to better match ab initio torsion profiles. The details of the lipid force field modification are given in the Supporting Information (SI) with area per lipid and torsion fitting results presented in Figures S1 and S2 (SI), respectively. The CHEQ polarizable force field model for methyl guanidinium was constructed by adapting the CHARMM CHEQ force field for proteins,[46,58] extending the electrostatic parameters, hardnesses, and electronegativities from the protein force field for an arginine side chain. We stress that we perform all simulations in the NP_AT ensemble.

The methyl guanidinium was partitioned into two charge normalization units to control polarizability scaling. The first unit encompasses the methyl ($-CH_3$) and secondary amine ($-NH$) groups, while the second unit includes the central carbon and two primary amine groups ($-C(NH_2)_2$). This

dx.doi.org/10.1021/jp400389z | J. Phys. Chem. B 2013, 117, 3578–3592

Table 1. Hydrogen Bond Distances and Interaction Energies between Methyl Guanidinium and Lipid Headgroup Analogue Molecules Dimethyl Phosphate (DMP) and Tetramethyl Ammonium (TMA), Water, and Chloride Calculated Using the CHARMM CHEQ Force Field (FF)[a]

molecule	q (e)	H-bond type	R^{FF}_{H-X} (Å)	R^{QM}_{H-X} (Å)	$E^{FF}_{interaction}$ (kcal/mol)	$E^{QM}_{interaction}$ (kcal/mol)
DMP	−1	H_2NH-O	1.69	1.57	−113.73	−120.33
		H_2NH-O	1.69	1.60		
TMA	+1	−	−	−	58.67−14.46	51.94
water	0	H_2NH-O	2.18	2.02	−12.82	−16.57
		H_2NH-O	2.18	2.00		
		$NH-O$	2.31	2.00	−12.00	−16.42
		H_2NH-O	2.10	2.02		
		H_2NH-O	2.02	1.83	−11.80	−13.39
		H_2CH-O	2.83	2.76		
		H_2CH-O	2.83	3.00		
chloride	−1	H_2NH-Cl	2.30	1.96	−93.62	−114.55
		H_2NH-Cl	2.31	2.01		
		$NH-Cl$	2.36	1.92	−92.19	−112.32
		H_2NH-Cl	2.26	2.05		
		H_2NH-Cl	2.18	1.70	−91.63	−115.63
		H_2CH-Cl	2.92	3.07		
		H_2CH-Cl	2.92	2.74		

[a]Quantum mechanical (QM) interaction energies were calculated at the MP2/aug-cc-pvtz level of theory using counterpoise correction. All QM calculations were carried out using the Gaussian 03 package.[93] The H-bond type indicates the specific atoms involved to differentiate between methyl guanidinium hydrogens belonging to NH_3, NH, and CH_3 groups. The range in values given for the mguan/TMA FF interaction energy represents the variation in the interactions found given distance separations (measured between the central carbon of $mguanH^+$ and the central nitrogen of TMA) from 5.7 to 22.7 Å between the two like-charged species, while the QM interaction is for an analogous structure with a separation of 6.1 Å. The three values given for the interaction energies between $mguanH^+$ and both water and chloride represent three unique and stable geometries around methyl guanidinium.

partitioning allows for consistency with the existing CHARMM CHEQ protein force field and permits use of the existing nonbond (LJ and electrostatic) parameters for arginine from the polarizable force field. The partitioning approach has been applied previously by our group in the treatment of proteins, lipids, and carbohydrates.[52−54,57,71,80,81] The isotropic, gas-phase molecular polarizability for this molecule was determined to be 6.4 $Å^3$ compared to the value of 7.0 $Å^3$ from MP2/aug-cc-pVTZ calculations. A reduction in the force field molecular polarizability is consistent with the decrease in the intrinsic molecular polarizability observed, in theory, when going from the gas to the condensed phase. However, the exact magnitude of this reduction is currently unknown and poses a challenge for force field development. We consider only the protonated methyl guanidinium model compound for our studies. Recent studies[2,9,82] have explored the shift in stability of the protonated and unprotonated species, as manifested in pK_a shifts, along the bilayer normal. For thin membranes, it has been suggested that the protonated state is plausible and sustained by a combination of lipid membrane deformation and long-lived polar (water and lipid) pores across the bilayer stabilizing the charge. Acknowledging these studies, we focus here on the free energetics of partitioning of the charged species.

The nonbonded (Lennard-Jones) interactions between methyl guanidinium and lipid headgroup analogues dimethyl phosphate (DMP) and tetramethyl ammonium (TMA), as well as with solvent species (water and chloride), were validated through the comparison of gas-phase small-molecule geometries and interaction energies calculated using the CHEQ force field with those calculated using high-level quantum mechanics. All quantum mechanical (QM) dimer structures were optimized at the MP2/aug-cc-pVTZ level with the exception of the $mguanH^+$/DMP dimer, which was optimized using the 6-31++g(2d,p) basis set. Interaction energies were calculated at the MP2/aug-cc-pVTZ level using the previously optimized structures. Hydrogen bond distances and interaction energies are shown in Table 1, and although overestimated, the hydrogen bond distances exhibit suitable agreement between the force field and MP2/aug-cc-pVTZ optimized structures. Interaction energies are consistently underestimated but are in fair agreement with QM values. In the absence of laborious reparameterization of the methyl guanidinium interactions with all system species, we consider it sufficient that for the purposes of the present work the trend of relative interaction strengths based on QM and force field calculations is equivalent, with the strongest interactions occurring between $mguanH^+$ and DMP.

C. Methyl Guanidinium Hydration Free Energy via Thermodynamic Integration. To further describe the quality of the present methyl guanidinium interactions with solvent, as well as to compare with existing literature data from earlier computational and experimental studies, hydration free energies of methyl guanidinium in dilute aqueous and hexane solutions were calculated using a cubic box of 988 TIP4P-FQ water molecules (or 216 hexane molecules) and one $mguanH^+$ molecule via thermodynamic integration (TI). Following the two-step decoupling procedure described by Warren et al. for single ion hydration,[83] the $mguanH^+$ is first electrostatically decoupled from the solvent followed by a decoupling of the nonbonded Lennard-Jones (LJ) interactions.

$$\Delta G^{TI}_{\lambda_1+\lambda_2} = \Delta G^{TI}_{\lambda_1} + \Delta G^{TI}_{\lambda_2} = \int_0^1 d\lambda_1 \left\langle \frac{dH(\lambda_1)}{d\lambda_1} \right\rangle_{\lambda_2=0} + \int_0^1 d\lambda_2 \left\langle \frac{dH(\lambda_2)}{d\lambda_2} \right\rangle_{\lambda_1=1} \quad (5)$$

dx.doi.org/10.1021/jp400389z | J. Phys. Chem. B 2013, 117, 3578−3592

where $H(\lambda)$ is the Hamiltonian for the system, while λ_1 and λ_2 are path coordinates for the electrostatic and LJ decoupling, respectively. This scheme allows for a complete decoupling of solute−solvent interactions while avoiding any errors arising from an exposed charge in the absence of any LJ repulsion. Double wide sampling (forward and reverse) is employed for both decoupling schemes to reduce sampling bias. Each λ window was sampled for a total of 225 ps of molecular dynamics, with the first 25 ps taken as equilibration and the last 200 ps considered for averaging. Simulations were performed in the NPT ensemble with a pressure of 1 atm and temperature of 323 K.

On the basis of well-established work regarding hydration free energies of ions in condensed phases using periodic Ewald-type methods, we consider corrections for the finite size of the simulation cells used in this work. We follow the results of Lynden-Bell.[84] For a cubic periodic simulation cell of edge length L, the reversible work to create a periodic lattice of charges (in this case the lattice of charges of the ion) in vacuum (relative dielectric of unity, $\varepsilon = 1$) is

$$\Delta = \frac{\xi q^2 e^2}{8\pi\varepsilon_0 L} \tag{6}$$

This equation represents the work in the potential of the periodic images of the central ion. The same process in a condensed-phase dielectric medium of relative dielectric constant ε is

$$\Delta = -\frac{\xi q^2 e^2}{8\pi\varepsilon\varepsilon_0 L} \tag{7}$$

Since we adopt the method of Warren and Patel for use with charge equilibration models, we dynamically remove the first contribution during the TI simulation process;[83] this leaves only the second term for consideration as the finite size correction in our case. We use $\xi = -2.837297$ for the lattice parameter, and the average box lengths (for NPT TI simulations) for water and hexane are $L_{water} = 31.1$ Å and $L_{hexane} = 37.0$ Å, respectively.

To account for nonbonded LJ interactions beyond the finite cutoff distance, a long-range correction is estimated, as described previously by Zhong et al.,[52] using an analytic repulsion−dispersion correction suggested by Shirts[85]

$$E_{LRC}(r_{ij}) = \sum_i \sum_j 16\pi\rho\varepsilon_{ij} \int_{r=r_{on}}^{\infty} \left[\left(\frac{\sigma_{ij}}{r_{ij}}\right)^{12} - \left(\frac{\sigma_{ij}}{r_{ij}}\right)^{6} \right] (1 - S(r_{ij}))r_{ij}^2 \mathrm{d}r \tag{8}$$

where i and j run over the solute and solvent atoms, respectively; ρ is the number density of the solvent molecules; ε_{ij} is the LJ well-depth; σ_{ij} is the solute−solvent effective LJ diameter; r_{on} is the separation at which the switching function activates; and r_{off} is the separation distance at which the LJ cutoff potential is zero (the switching function if zero). The switching function, $S(r_{ij})$, is defined in CHARMM as

$$S(r_{ij}) = \begin{cases} 1, & r_{ij} \le r_{on} \\ \dfrac{(r_{off}^2 - r_{ij}^2)^2(r_{off}^2 + 2r_{ij}^2 - 3r_{on}^2)}{(r_{off}^2 - r_{on}^2)^3}, & r_{on} < r_{ij} \le r_{off} \\ 0, & r_{ij} > r_{off} \end{cases} \tag{9}$$

We also add an a posteriori correction to account for contributions from the interfacial potentials of the air−water and air−-hexane interfaces. The interfacial potential of a system can be calculated through double integration of charge density as a function of distance from the center of the solvent layer along the interface normal[86]

$$V(z) = -\frac{1}{\varepsilon_0}\int_{\infty}^{z}\int_{\infty}^{z'} \rho(z'')\mathrm{d}z''\mathrm{d}z' \tag{10}$$

Here, ε_0 is the permittivity of the vacuum, and $\rho(z)$ is the charge density achieved by segmenting the system into slices of width dz and summing the charges within each slice.

D. Potential of Mean Force. To calculate the equilibrium potential of mean force (PMF) for methyl guanidinium traversing the lipid membrane, umbrella sampling windows were constructed along a reaction coordinate representing the z-component of the difference between the centers of mass of mguanH$^+$ and the lipid bilayer. Windows were constructed at 1 Å intervals in bulk solution (-35 Å $\le z \le -33$ Å) and 0.5 Å intervals at the water−lipid interface and in the interior of the membrane (-32.5 Å $\le z \le 0$ Å) for a total of 69 independent simulation windows. Each window was sampled for 10.0 ns. The weighted histogram analysis method (WHAM)[87] was used for postsimulation unbiasing. The center of mass restraint was imposed using the CHARMM miscellaneous mean field potential (MMFP) utility[88] and was continuously monitored to ensure sufficient overlap between adjacent windows. MguanH$^+$ motion in the lateral plane was not restrained; once within the bilayer interface, the lateral motion is effectively damped. To maintain the system geometry an additional planar restraint was enforced on the center of mass of the bilayer to prevent drift of the lipid in the z-direction. Initially, the mguanH$^+$ was placed in the bulk solvent region of a previously equilibrated DMPC/water simulation cell. From molecular dynamics simulations of unrestrained mguanH$^+$, we selected snapshots spanning a range of positions between the mguanH$^+$ and bilayer center of mass; this generated starting configurations at various z-positions in bulk (far from the bilayer−water interface) to positions in the vicinity of the interface. From umbrella sampling simulations in windows close to the interface, we selected a snapshot where the position of the mguanH$^+$ was in the window closer to the bilayer center and then began an umbrella sampling simulation in that window. After 1 ns of simulation in this window, we repeated the process for the remaining windows moving into the bilayer center. For each window, we allowed one nanosecond of equilibration before considering the rest of the simulation data as production data.

To independently confirm the PMF computed via umbrella sampling and WHAM unbiasing of probability distributions as well as establish a method to allow decomposition of the overall PMF into contributions from various system components (such as water, lipid, ions, etc.), we use a somewhat ad hoc force-based approach as follows. The force decomposition method and caveats related to the use of a lipid reference and cutoff

dx.doi.org/10.1021/jp400389z | J. Phys. Chem. B 2013, 117, 3578−3592

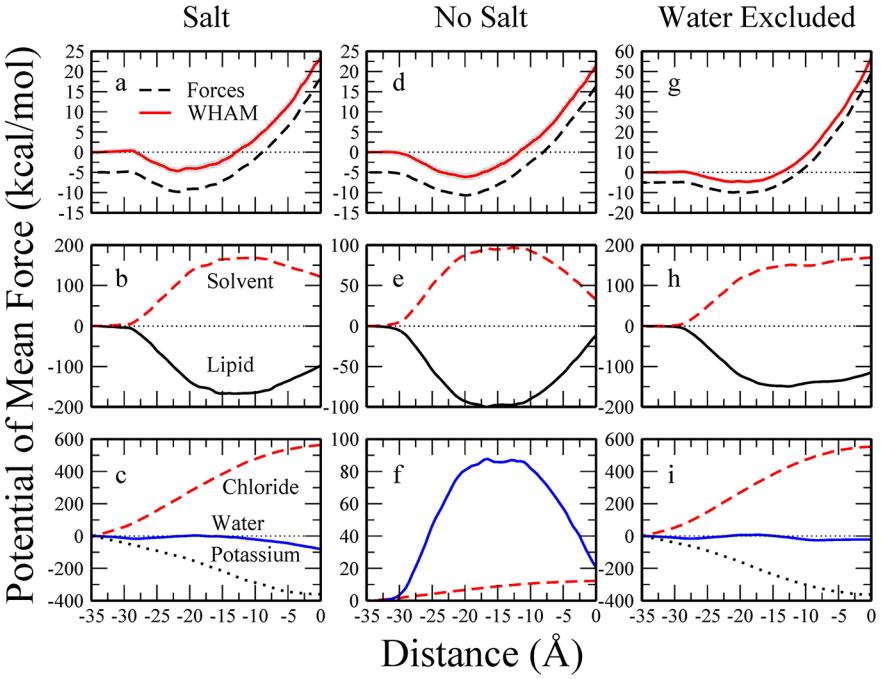

Figure 1. Decomposition of the potential of mean force for the Salt, No Salt, and Water Excluded systems. (a, d, g) The PMFs calculated via umbrella sampling with WHAM analysis as well as through integration of forces. The integrated force profiles have been offset by −5 Å for clarity. (b, e, h) Decomposition of the total PMF into solvent (red, dashed curves) and lipid contributions (solid, black curves). (c, f, i) Decomposition of the solvent contributions into constituent water (solid, blue curves), chloride ion (red, dashed curves), and potassium ion (black, dotted curves) contributions. Dotted lines at 0 were added to clarify positive and negative PMF contributions.

versus PME electrostatics have been discussed in detail by Li et al.,[2] and we refer the reader to that reference and the associated SI for relevant details. We compute the PMF defined as

$$\Delta W = -\int_{\zeta=-35}^{\zeta=0} \langle F_z(\zeta)\rangle \mathrm{d}\zeta \tag{11}$$

where ζ is the z-component of the center of mass distance between mguanH$^+$ and the lipid bilayer; $\langle F_z\rangle$ is the average force in the z-direction (normal or the bilayer) experienced by the mguanH$^+$ when it is at position ζ. The PMF represents the reversible work associated with changing the relative center of mass distance from a value of −35 Å (methyl guanidinium in bulk solution) to 0 Å (methyl guanidinium in bilayer center). Since we are using data from the harmonically restrained MD simulations (which allow a narrow Gaussian distribution of positions centered at the unique positions selected along the reaction coordinate), the average force along the reaction coordinate, $\langle F_z\rangle$, is not exactly associated with a unique value of the reaction coordinate but averaged over this narrow Gaussian distribution of positions; in this sense, we consider this an ad hoc approach. On the basis of the current results (and those published previously[49]), we see that both approaches lead to self-consistent results. Finally, we consider the total force acting on the methyl guanidinium as well as the decomposition of the total force into constituent contributions

$$\begin{aligned}\Delta W &= \Delta W_{\mathrm{Lipid}} + \Delta W_{\mathrm{MguanH^+}} + \Delta W_{\mathrm{Solvent}} \\ &= -\int_{\zeta=-35}^{\zeta=0} \langle F_{z,\mathrm{Lipid}}(\zeta)\rangle \mathrm{d}\zeta - \int_{\zeta=-35}^{\zeta=0} \langle F_{z,\mathrm{MguanH^+}}(\zeta)\rangle \mathrm{d}\zeta \\ &\quad - \int_{\zeta=-35}^{\zeta=0} \langle F_{z,\mathrm{Solvent}}(\zeta)\rangle \mathrm{d}\zeta\end{aligned} \tag{12}$$

where the solvent contribution can be further decomposed into water and inorganic ion (potassium and chloride ion) contributions

$$\begin{aligned}\Delta W_{\mathrm{Solvent}} &= \Delta W_{\mathrm{Water}} + \Delta W_{\mathrm{Potassium}} + \Delta W_{\mathrm{Chloride}} \\ &= -\int_{\zeta=-35}^{\zeta=0} \langle F_{z,\mathrm{Water}}(\zeta)\rangle \mathrm{d}\zeta \\ &\quad - \int_{\zeta=-35}^{\zeta=0} \langle F_{z,\mathrm{Potassium}}(\zeta)\rangle \mathrm{d}\zeta \\ &\quad - \int_{\zeta=-35}^{\zeta=0} \langle F_{z,\mathrm{Chloride}}(\zeta)\rangle \mathrm{d}\zeta\end{aligned} \tag{13}$$

To investigate the effect of the inorganic ion concentration on the PMF, we construct a KCl-free mguanH$^+$−lipid system in pure water. This No Salt system is similar to the 1 M KCl Salt system described previously except that all of the inorganic ions have been removed (except one Cl^- to maintain charge neutrality). A series of umbrella sampling windows were constructed analogous to those of the Salt system (69 total), and MD simulations were run for 10 ns.

To study the importance of continuous solvation on the ability of mguanH$^+$ to penetrate the bilayer and its ramifications on the PMF for permeation, we construct a Water Excluded system, analogous to the 1 M KCl Salt system, with an added restraint to prevent water from entering the center of the membrane. The planar restraint was added using the MMFP utility which imposes a penalty function to prevent water from penetrating the lipid further than ±12 Å from the membrane center in the z-direction. This effectively dehydrates the lipid below the carbonyl groups and prevents mguanH$^+$ from bringing any solvating water molecules into the membrane. Umbrella sampling windows were constructed similar to the

dx.doi.org/10.1021/jp400389z | J. Phys. Chem. B 2013, 117, 3578−3592

previous systems but with additional windows spaced at 0.25 Å intervals added in the lipid interior (-4.75 Å $\leq z \leq 0$ Å). Higher harmonic force constants were required due to the difficulty of generating adjacent windows at distances further then 0.25 Å while approaching the center of the membrane. Each window of the Water Excluded system (79 total) was run for 10 ns of production.

Uncertainty estimates for the WHAM-based PMF are determined using eq 1 of Zhu and Hummer;[89] variances needed for this method were obtained using the blocking method of Flyvbjerg et al.[90] The PMF was considered converged once the uncertainty of the PMF at various positions along the reaction coordinate reached a plateau value.

III. RESULTS AND DISCUSSION

A. Hydration Free Energies. Correction factors for the long-range LJ interactions (past the finite cutoff) for the mguanH$^+$/water and mguanH$^+$/hexane systems were calculated to be -0.90 and -5.52 kcal/mol, respectively. The interfacial potential of TIP4P-FQ water (at 323 K) was previously found to be -12.45 kcal/mol,[50] while that of hexane (at 298 K) was found to be -4.12 kcal/mol.[91] We assume that the interfacial potential of hexane will not change significantly within the temperature range of 298–323 K. Taking into account the correction factors results in a hydration free energy for mguanH$^+$ in pure TIP4P-FQ (air to water) to be -57.91 ± 0.09 kcal/mol and that of mguanH$^+$ in pure hexane (air to hexane) to be -23.64 ± 0.05 kcal/mol which results in a partitioning free energy (water to hexane) of 34.27 ± 0.07 kcal/mol. These values compare fairly well with those of Vorobyov et al. using Drude polarizable force fields in which the authors find the hydration free energies for mguanH$^+$ in water and in hexane to be -61.72 ± 0.09 and -27.54 ± 0.16 kcal/mol, respectively, and an overall partitioning free energy (water to hexane) of 34.69 ± 0.19.[3] The lower value we find for the hydration free energy of mguanH$^+$ in TIP4P-FQ water may be related to the underestimated interaction energy found using the CHEQ force field versus quantum mechanical calculations.

B. Salt PMF. Figure 1a shows the total PMF based on umbrella sampling (red, solid curve) and integrated force (black, dashed curve) for mguanH$^+$ traversing the lipid bilayer; the dashed curve is shifted by -5 kcal/mol for clarity. Uncertainties are shown in panels a, d, and g (see also SI Figure S10 and discussion of uncertainty calculations and Figure S11 for assessment of convergence of PMF). The PMF shows a minimum of -4.6 kcal/mol (relative to bulk water) in the region of the lipid headgroups. The stability of methyl guanidinium near the lipid headgroups has also been observed in simulations of an unrestrained mguanH$^+$ which crosses the bilayer–water interface and preferentially resides in the headgroup region (see SI and Figure S3 therein). The barrier reaches a peak of around 28 kcal/mol (relative to the global minimum in the headgroup region) at the center of the membrane. This barrier is about 5–10 kcal/mol higher than, but reasonably consistent with, previous results using polarizable, nonpolarizable, and coarse-grained force fields to simulate the transfer of guanidinium, methyl guanidinium, propyl guanidinium, and an exposed arginine attached to a polyleucine α helix across a lipid membrane.[1−5] Though plausible to suspect that polarizability of the lipids, leading to a dielectric constant of 2 (versus 1 for additive force fields),[92] would give rise to a smaller difference between the bulk/minimum and bilayer center, we draw attention to other factors contributing to the free energetics. First, the balance between solvent–mguan and headgroup–mguan interactions may not be accurate (though compared here to quantum mechanical calculations at the correlated level). However, based on the underestimation of the interaction of the mguanH with the negatively charged component of the headgroup, and the repulsive interaction between the like-charged tetramethyl guanidinium group, we believe that an imbalance would work to lower the barrier. Second, the dipole potential for our charge equilibration model has been determined to be higher by about 200 mV compared to fixed-charge, additive force fields,[54,57] though the underlying assumptions invoked in determination of canonical experimental values remain ambiguous;[50] this would lead to a slightly higher barrier for a positively charged molecule as in this case. Finally, the difficult issue of the deformation energy of the membrane may also be at play. As discussed below, the bilayer is deformed to some extent in the permeation process, and the various properties of the bilayer (rigidity, headgroup–headgroup interactions, etc.) are possibly different in this model compared to the general additive, fixed-charge model. Thus, we do not consider that the polarization of the lipid chains is a sole contributor to any effects on the barrier height; this is a result of several contributions, only a few of which have been addressed in the preceding discussion.

To elucidate in more detail specific contributions from system components to the total PMF (i.e., water, ions, lipids, solvent, and lipid buried in the bilayer center in the vicinity of the permeating cation, etc.), we consider individual contributions next. This analysis also provides information useful in comparing contributions from system elements based on simulations using nonpolarizable force fields or continuum dielectric based methods (implicit solvent or lipid models). The decomposition of the integrated force PMF (Figure 1b) shows that the stabilizing contribution of the lipid (solid, black curve) is offset by the slightly more destabilizing contribution from the solvent (red, dashed curve). After further decomposition (Figure 1c) of the solvent, the destabilizing contribution arises solely from chloride (red, dashed curve). The water (solid, blue curve) and potassium (dotted, black curve) contributions are stabilizing but not sufficiently adequate to balance the large (about 560 kcal/mol) chloride contribution. The slopes of the profiles are indicative of the sign (direction) of the z-component forces acting on mguanH$^+$ at varying distances from the center of the bilayer. The total lipid contribution is increasingly stabilizing as the mguanH$^+$ travels into the membrane headgroup region from the bulk, reaching a plateau from about -15 to -10 Å (in the area of the lipid carbonyls), and becomes less stabilizing as mguanH$^+$ approaches the membrane center; a large destabilization (positive slope leading to negative z-direction forces) arises from the large electrostatic forces of the headgroups and carbonyl moieties of distant lipids attracting the positively charged cation. Similar but opposite behavior is seen with the solvent contribution which is increasingly destabilizing moving from the bulk and into the membrane interface, plateauing in the carbonyl region, and becoming less destabilizing toward the center of the bilayer due to the increased stabilization from water solvating mguanH$^+$ at the center of the membrane. The ion contributions show fairly linear behavior from the bulk and into the lipid, reaching a plateau toward the center of the membrane where the force of the ions on mguanH$^+$ will be minimal. We observe over the course of the simulation that, for the window in which the mguanH$^+$ is in the center of the bilayer ($z = 0$), there is at least

one lipid phosphate group strongly associating with the mguanH$^+$ 94% of the time as well as several water molecules (1 to 7 on average, and up to 12 in rare instances) surrounding it. We define a lipid or water molecule as strongly associating if the lipid phosphate or water oxygen atoms are within 5 Å of the mguanH$^+$ center of mass. Coordination profiles and histograms are presented in Figure 2. The profile showing the number of

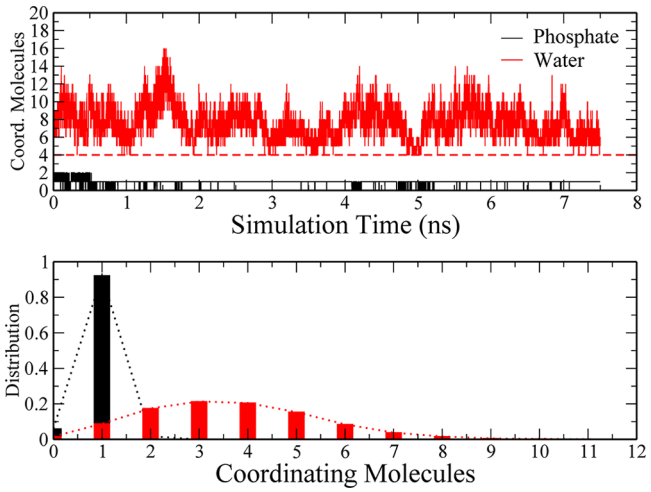

Figure 2. Number of coordinating lipid phosphate (black) and water (red) molecules surrounding methyl guanidinium (within 5 Å of the mguanH$^+$ center of mass) at the center of the lipid membrane as a function of simulation time (top) and as a distribution over all data (bottom) for the Salt system. The number of coordinating water molecules (top, red profile) has been offset by 4 for clarity with the dashed red line indicating zero.

coordinating water molecules as a function of time (top, red profile) has been offset by 4 for clarity with a dashed red line added to indicate zero. Our results are in qualitative agreement with the solvation profiles observed for mguanH$^+$ in the work of Li et al.[2] We will consider the nature of the water contributions in the various systems (as shown in Figure 3) further below.

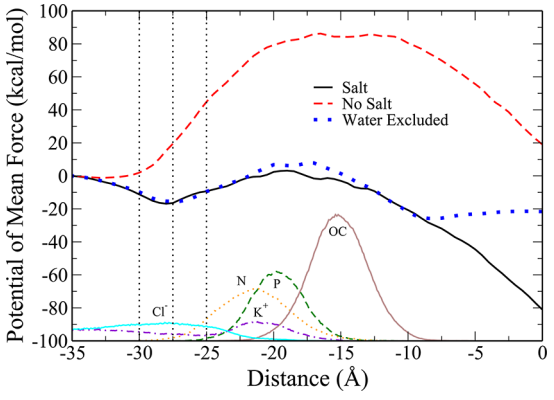

Figure 3. Comparison of the water contributions to the total PMF profiles of the Salt, No Salt, and Water Excluded systems. Number density profiles for select lipid and salt atoms, taken from the Salt system in which methyl guanidinium is in the bulk (z = −35 Å), are shown to give a sense of the lipid environment. Vertical dotted lines were added to distance values of −30, −27.5, and −25 Å to guide the reader during the discussion in the main text.

C. No Salt PMF. The large and sole destabilizing contribution of the chloride anions to the total PMF leads us to explore the effects of ion concentration on the free energetics of mguanH$^+$ permeation into the bilayer; we thus consider the extreme case of zero salt concentration. Figure 1d shows the total PMF profiles (WHAM-based and integrated forces) for the No Salt system, which is similar in shape and magnitude with the PMF of the Salt system; the black dashed line is the result of the force-based PMF, shifted by −5 kcal/mol for clarity. A global minimum of −5.7 kcal/mol is seen in the headgroup region of the lipid, similar to the −4.6 kcal/mol minimum found in the Salt system. This slight (1.1 kcal/mol) difference may be caused by the accessibility of additional mguanH$^+$ bonding sights in the lipid that had previously been occupied by potassium ions. Taking into account the slightly deeper minimum we see a barrier peak of about 28 kcal/mol at the center of the membrane, consistent with the Salt system. To demonstrate that an absence of ions will have no affect on the overall lipid structure, we compare heavy atom number density profiles between the Salt and No Salt systems, with details and results shown in the Supporting Information, Figure S4.

The similarities between Salt and No Salt systems are intriguing due to the very large contributions that the ions have in the total Salt PMF. To further explore this we decompose the PMF into constituent contributions, as done for the Salt system, via eqs 12 and 13 with results shown in Figure 1e and f. As in the Salt system, the favorable lipid contribution (solid, black curve) is offset by an unfavorable solvent contribution (red, dashed line). While the overall shape and sign of the contribution profiles resemble that of the Salt system we note that the magnitude of the lipid and solvent interactions is much lower at the center of the bilayer in the system without salt. Further decomposition of the solvent contributions (Figure 1f) shows that the single chloride ion (red, dashed line) destabilizes the system by 12.5 kcal/mol. That the forces from the single chloride are indeed destabilizing (i.e., in the negative z-direction) while the methyl guanidinium is asymmetrically positioned in the negative side of the bilayer is demonstrated in Figure S5 of the SI. Water (solid, blue line), having been stabilizing for the Salt system (−81 kcal/mol), now exhibits a destabilizing contribution of about 20.5 kcal/mol at the center of the bilayer. The slopes of the lipid and solvent profiles are similar with those of the Salt system with the lipid contribution increasingly stabilizing from the bulk to the headgroup region, reaching a plateau from around −17.5 to −12.5 Å (slightly closer to the bulk region than in the Salt system) and becoming less stabilizing toward the center of the membrane. The solvent contribution is increasingly destabilizing until reaching a plateau and becoming less destabilizing approaching the membrane center. The water contribution, which comprises the majority of the solvent contribution, is increasingly destabilizing, moving from the bulk toward the lipid and upon entering the membrane reaching a plateau (similar to that of the solvent and lipid contributions) before becoming less destabilizing toward the center of the membrane. This behavior is starkly different from the water contribution in the system with salt; we address possible origins of this difference in Section IIIE.

D. Water Excluded PMF. We have seen that mguanH$^+$ is able to deform the membrane while remaining solvated by several water molecules which serves to stabilize the cation in the center of the membrane. We investigate the effects of removing this stabilizing water by excluding water from the center of the membrane and effectively dehydrating mguanH$^+$

dx.doi.org/10.1021/jp400389z | J. Phys. Chem. B 2013, 117, 3578−3592

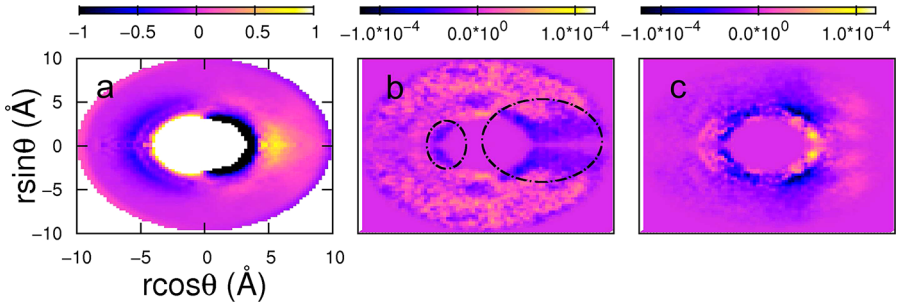

Figure 4. Panel a shows the force from water molecules at different positions around a centered methyl guanidinium when the cation is in the umbrella sampling window at −30.0 Å relative separation. Shown are results for the Salt system, with analogous profiles for the No Salt systems (shown in the Supporting Information). Positive forces (lighter color) bias the cation toward the bilayer center (positive z-direction), and negative forces (darker color) bias the cation toward the bulk solution (negative z-direction). Panel b shows difference in local water density between the No Salt and Salt systems where positive values correspond to a higher local water density in the No Salt system relative to the Salt system; negative values correspond to the opposite. Panel c shows the difference in density-weighted force, $\Delta F_\rho = F_\rho(\text{No Salt}) - F_\rho(\text{Salt})$ at −30 Å.

and the lipid headgroups that form the lipid deformation. The resulting umbrella sampling and force-based PMFs for the Water Excluded system are shown in Figure 1g, the shape of which shows a much steeper rise, starting at around $z = -15$ Å (near the lipid carbonyl groups), than the PMF profiles for the Salt and No Salt systems. The PMF reaches a peak value of about 66 kcal/mol (relative to the global minimum of −4.7 kcal/mol in the headgroup region) at the center of the bilayer, more than twice as high as those found for the Salt and No Salt systems in which water is allowed to permeate the membrane and continuously solvate mguanH$^+$ and any lipid headgroups accompanying the cation into the bilayer.

Decomposition of the PMF into solvent and lipid contributions shows that, as in the Salt and No Salt systems, the solvent contribution is strongly destabilizing while the lipid contribution is stabilizing but not strong enough to offset the solvent. Decomposition of the solvent contributions shows similarities with the Salt system, in that the chloride contribution is the only destabilizing species, while the lipid, water, and potassium all stabilize the mguanH$^+$ in the center of the bilayer.

E. Water Contribution to Total PMFs. After decomposing the PMFs of the three systems above we find that the water contribution profiles for the 1 M systems (Salt and Water Excluded) are quite similar with one another (at least until the region where the planar water constraint takes effect), while that of the No Salt system is markedly different in magnitude and somewhat in shape. In particular, the water contribution for the Salt system shows that the water is initially stabilizing as the mguanH$^+$ enters the bilayer, a behavior which is not observed for the system devoid of salt. This is apparent in the direct comparison of the three water contribution profiles shown in Figure 3. Number density profiles for select lipid atoms (taken from a Salt system window where methyl guanidinium was in the bulk) are shown to help illustrate the various regions of the membrane. We show in the SI (Figure S4) that the average lipid component distributions are similar for the Salt and No Salt systems. It is plausible to consider that differences in local water density around mguanH$^+$ entering the bilayer may lead to different net forces, stabilizing the cation in one high salt concentration case. We next consider local hydration and its consequences. Since the biggest difference in the water contributions to the PMF occur at −30 Å (Figure 3, the slopes are of opposite sign) we consider this position in detail.

To investigate the difference in the water contributions to the total PMF of the Salt and No Salt systems we analyze the forces that individual water molecules in the local hydration environment (within 10 Å from the mguanH$^+$ center of mass) of mguanH$^+$ exert on methyl guanidinium. We are interested in mapping the direction and magnitude of the z-component of force on mguanH$^+$ from a water molecule at a particular position around the cation. The reference coordinate system we choose to represent the relative position is a spherical polar coordinate system. We first define a vector $\vec{r}_{\text{cation,water}}$ between the center of mass of the methyl guanidinium and the water molecule under consideration. The angle between the z-axis of the overall system and this vector is taken to be θ, and the angle between the x-axis and the projection of $\vec{r}_{\text{cation,water}}$ onto the $x-y$ plane is taken to be ϕ. We can thus consider the z-direction force on methyl guanidinium arising from a water molecule at a relative position defined by $|\vec{r}_{\text{cation,water}}|,\theta,\phi$ as $F_z(|\vec{r}_{\text{cation,water}}|,\theta,\phi)$. For visualization of the position-dependent force on methyl guanidinium from hydration water molecules, we choose to plot in ensuing figures F_z as a function of the angle θ by essentially averaging over the $x-y$ plane angle ϕ. We use two more mappings related to the angle θ. First, the z-position of the water molecule relative to the methyl guanidinium center of mass is simply $z = |\vec{r}_{\text{cation,water}}| \cos(\theta)$. Thus, plotting with $|\vec{r}_{\text{cation,water}}| \cos(\theta)$ as one axis of the figure gives information on the z-position of the water molecule. Second, the distance in the $x-y$ plane from the center of mass of methyl guanidinium to the water molecule is simply $|\vec{r}_{\text{cation,water}}| \sin(\theta)$; thus, we choose this distance as the second axis in our ensuing figures.

Forces were calculated using CHARMM with PME (the same grid size used for full bilayer simulations). Coordinate files were extracted from trajectories, and all lipid, salt, and water (with any atoms outside of 10 Å from the methyl guanidinium center of mass) were deleted. The force from individual water molecules was calculated by looping through the remaining water molecules and calculating the position of the water and the total force on the cation. We correct for the force of methyl guanidinium on itself by deleting all water molecules and calculating the force on the cation in isolation; this captures the forces on the single cation in the central simulation cell from intramolecular interactions as well as it periodic images. Extracting the forces exerted by water molecules surrounding methyl guanidinium allows us to map the variation between contributions from first and higher solvation shell waters as well

dx.doi.org/10.1021/jp400389z | J. Phys. Chem. B 2013, 117, 3578−3592

as show at which positions water will have a stabilizing or destabilizing effect. We analyze the final 3 ns of data from several umbrella sampling windows for both the Salt and No Salt systems. To account for differences in water density between windows and between Salt and No Salt systems, we weight the forces by the density of water (relative to the total number of water molecules sampled surrounding mguanH$^+$), $F_\rho = (F(z))(\rho_{water}(z))$.

To address local water density differences and the resulting differences in net force from local water molecules on mguanH$^+$ at z = 30 Å, we compute maps of the water density difference ($\Delta\rho$) and density-weighted force difference (ΔF_ρ) between the two systems in Figure 4. Explicitly, $\Delta\rho = \rho$(No Salt) − ρ(Salt) and $\Delta F_\rho = F_\rho$(No Salt) − F_ρ(Salt) .

Figure 4a shows the force from water molecules at different positions around a centered methyl guanidinium when the cation is in the umbrella sampling window at −30.0 Å relative separation. Shown are results for the Salt system, with analogous profiles for the No Salt systems (shown in the Supporting Information). Positive forces (lighter color) bias the cation toward the bilayer center (positive z-direction); negative forces (darker color) bias the cation toward the bulk solution (negative z-direction). We note some general characteristics. At points closest to the cation (regardless of the ϕ angle in the x–y plane), water contributes a repulsive force. Thus, a first-solvation layer water molecule on the bulk solution side of the cation center of mass (COM) will stabilize the cation toward the center (as evidenced by the light color), and a first-solvation layer water molecule on the bilayer center side will push the cation toward the bulk (dark color). Water molecules in second and higher solvation shells generally attract the cation in opposition to first solvation layer molecules.

The difference in local water density between the No Salt and Salt systems is shown in Figure 4b where positive values correspond to a higher local water density in the No Salt system relative to the Salt system; negative values correspond to the opposite. At a position of −30.0 Å, the Salt system has higher water density on the bilayer-center side of the methyl guanidinium center of mass (circle on right); this region would contribute stabilizing forces on the cation, and the position of −30.0 Å corresponds to the biggest difference in the water contribution behavior; that is, the slopes of the water contributions to the PMF are opposite.

Figure 4c shows the difference in density-weighted force, $\Delta F_\rho = F_\rho$(No Salt) − F_ρ(Salt). At −30 Å, the majority of regions of negative values suggests that the Salt system is contributing more stabilizing forces (net force that is more positive than in the No Salt system). This corresponds to the negative slope in the Salt system's water contribution to the PMF in this region (Figure 3). The origin of this singular difference comes from the interplay of water density differences and position-dependent forces around the cation in this region. Figures S6b and S7b in the Supporting Information show that the position-dependent z-direction forces ($F(z)$) for the Salt and No Salt system are similar. The densities (Figures S8b and S9b, SI) exhibit differences in the regions corresponding to both stabilizing and destabilizing forces in both systems. Comparing Figures S8b and S9b (SI) shows that in the Salt system local water density is higher at positions where water contributes forces that tend to stabilize the cation in the bilayer as reflected in the density difference, Figure 4b. In Figure 4b, the Salt system has higher density for z-positions between −3 and −4 Å from the center of mass of the cation (left circle); there is also higher water density in the Salt system for positions from 3 to 10 Å and $|\vec{r}_{cation,water}|\sin(\theta)$ values of ±5 Å. From Figure 4 and Figures S6b and S7b in the SI, water molecules in these regions exert stabilizing forces (toward the bilayer center) except for the small region between $|\vec{r}_{cation,water}|\cos(\theta)$ values of 3 and 5 Å. Effectively, the reduced density of water in the No Salt system in the locations where water exerts forces to pull the cation toward the center leads to the dramatic differences in the water contributions to the PMF. Moreover, this effect is local.

The higher local water density in the Salt system correlates with the position of the chloride anion density profile. Because the chloride prefers to be hydrated by either water or polar headgroups, it is reasonable that chloride anions bring with them water molecules to some extent. The chloride anion density reaches a maximum around −27.5 Å which corresponds to the minimum in the water contribution to the PMF. Thus, as methyl guanidinium enters the bilayer, as long as there is a local stabilizing asymmetry in water density, brought about by the asymmetry in the chloride anion density, the water contribution to the PMF is stabilizing. For methyl guanidinium residing at positions between 0 and −27.5 Å, since the chloride anion density is increasing toward the bilayer, thus increasing the stabilizing water density, the water contribution to the PMF is stabilizing. Moving further into the bilayer, the same water molecules now become destabilizing, thus giving rise to the barrier before finally becoming stabilizing at the bilayer center.

F. Core Lipid Headgroup and Water Contributions. To address the change in the slopes of the profiles for the lipid and water contributions to the total PMF (Figure 1) as the core region of the bilayer is encountered, we explore the energetics toward the center of the bilayer, in the "core" of the membrane. A water or lipid headgroup is considered to be in the core if a water oxygen or lipid phosphorus has a magnitude of |z|-position ≤ 13 Å. In Figure 5, for the Salt and No Salt systems we find similarly shaped profiles. The core water contribution is negligible, while mguanH$^+$ is in the bulk and becomes destabilizing as it approaches the carbonyl groups, with water molecules forced into the membrane center interacting with mguanH$^+$ presenting an effective "barrier" as these water

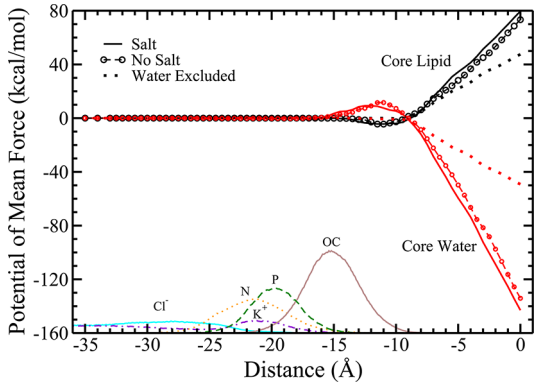

Figure 5. Decomposition of the potential of mean force into "core" lipid and water contributions for the Salt (black, solid curve), No Salt (red, dashed curve), and Water Excluded (blue, dotted curve) systems. Water or lipid molecules are defined as being in the membrane "core" if the water oxygen or lipid phosphorus has a |z|-position ≤ 13 Å. Scaled number density profiles for select lipid and salt atoms, taken from the Salt system in which methyl guanidinium is in the bulk (z = −35), are included to give a sense of the lipid environment, similar to those in Figure 3.

dx.doi.org/10.1021/jp400389z | J. Phys. Chem. B 2013, 117, 3578−3592

molecules prefer to remain in the polar environment of the carbonyl region. As mguanH$^+$ moves past the carbonyl groups, dragging lipid phosphates into the center of the membrane, the solvating water mainly exists in the region of the lipid deformation and yields an increasingly stabilizing contribution of about 140 kcal/mol. This effect has been observed by Li et al.[2] though to a lesser extent based on Figure 7 of ref 2 as well as Figures S4A and S4B of the associated Supporting Information. The lipid contribution is slightly stabilizing as the lipid phosphate groups pull mguanH$^+$ into the membrane but becomes increasingly destabilizing as mguanH$^+$ moves to the other side of the phosphate groups, pulling them into the membrane, and forming a deformation of the membrane. This is qualitatively similar to what is observed by Li et al.[2] The overall profiles for the core lipid molecules are strongly destabilizing (about 80 kcal/mol), while core water molecules are strongly stabilizing (about −140 kcal/mol).

Our results compare with the results of Li et al.[2] using nonpolarizable force fields. They find the core lipid, while still destabilizing (nearly 50 kcal/mol), is more than offset by the contribution from core water of about −90 kcal/mol leading to about 60 kcal/mol barrier from the partitioning of the cation into the unperturbed low dielectric bilayer and electrostatics of bulk electrolyte. We obtain a remainder contribution (result of subtracting the core lipid and water contributions from the total PMF) of about 80 kcal/mol. The higher barrier may arise from the higher dipole potential contribution of the polarizable bilayer model (1 V) as well as membrane properties such as rigidity and headgroup−headgroup interactions being different across force fields. Finally, in the Water Excluded system, we find that water within 13 Å of the bilayer center stabilizes the cation to a lesser degree, naturally due to the lesser number of water molecules in this region due to the restraint. The Water Excluded system shows a core water contribution strictly due to the definition we adopt (to be consistent with previous studies); had we chose the "core" water molecules to be within 12 Å of the bilayer center, then there would be no contribution since the restraints would not allow any water in this region; thus the "core" water contribution in the Water Excluded system arises solely from water molecules in a region from [−13,−12] and [12,13] Å from the bilayer center.

G. Water Defect Mediated Lipid Deformation. Finally, to investigate the role of water penetration in the lipid deformation process we constructed a system in which the mguanH$^+$ was generated and held at the center (z = 0) of the lipid bilayer, as opposed to slowly crossing down from bulk solution and through the lipid. A harmonic constraint was used to hold the mguanH$^+$ at the center of the bilayer, while a planar constraint, analogous to the one used in the Water Excluded umbrella sampling windows, prevents water from entering into the hydrophobic core of the membrane. This prevents the mguanH$^+$ from being solvated at any point during the simulation. Four replicate systems were run for around 27 ns each. We find that, over the course of the replicate simulations and in the absence of water penetration into the bilayer, the lipid headgroups do not deform to associate with the mguanH$^+$. To test if the structure of the bilayer is truly unperturbed while mguanH$^+$ is at the center of the membrane, we compare the heavy atom density profiles and headgroup orientation (P−N angle) with those of the umbrella sampling window in which the mguanH$^+$ is located in bulk water (z = −35 Å), with results of this comparison shown in Figure 6. The number density profiles and P−N angle distributions show that the structure of

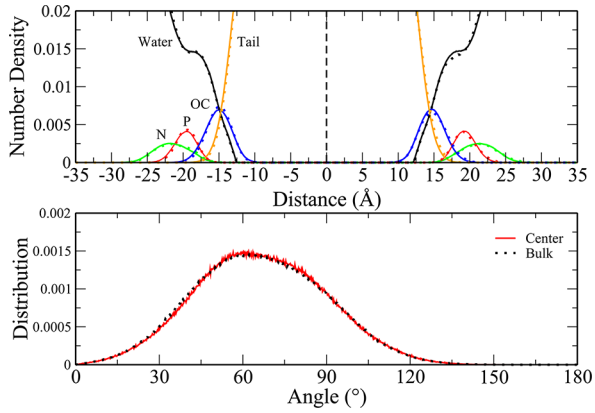

Figure 6. (Top) Heavy atom number density profiles for selected components (water oxygen, lipid headgroup phosphorus, and nitrogen, lipid carbonyl oxygen, and aliphatic lipid tail carbon) of the systems with a water constraint. The membrane-centered methyl guanidinium (with unperturbed lipid) profiles are shown as solid curves, while the profiles for the system with methyl guanidinium located in bulk water (z = −35 Å) are shown as dotted curves. The black dashed line represents the center of the bilayer (z = 0 Å). (Bottom) Distribution of the headgroup orientation measured as the angle between the P−N dipole vector and the bilayer normal (z-axis) for membrane centered (red curve) and bulk (black, dotted curve) mguanH$^+$.

the lipid membrane with mguanH$^+$ in the center remains intact and is comparable with that of the Water Excluded umbrella sampling window with mguanH$^+$ in the bulk solvent.

After several nanoseconds of dynamics on the Water Excluded, unperturbed systems, coordinate snapshots were extracted and used to create four replicate systems in which the water constraint was subsequently removed. We find that within a nanosecond water begins to penetrate the membrane to solvate the mguanH$^+$. Once water is allowed to flow into the membrane we see both lipid deformation and the penetration of chloride ions into the bilayer. Three of the replicates see a chloride ion (or ions) associating with the mguanH$^+$ before the lipid phosphate can move into the center of the bilayer. Lipid phosphate then replaces the chloride in associating with the mguanH$^+$ after several nanoseconds. The other replicate shows immediate membrane deformation with the lipid phosphate associating with the mguanH$^+$ shortly after water begins to surround the arginine analogue and stays as such throughout the simulation.

To explore this further we measure the distance between the center of mass of the mguanH$^+$ and the associating chloride and lipid phosphorus atoms as a function of time for each of the four replicates, with the results shown in Figure 7. Histograms of the number of associating species are shown below the distance profiles to indicate when a chloride (black) or lipid phosphorus (red) atom is within 5 Å of the mguanH$^+$ center of mass. Chloride profiles and histograms have been shifted by 30 Å for clarity. We find that, in all of the cases in which chloride penetrates the membrane and associates with the mguanH$^+$, the chlorides are originally in bulk solution and quickly move through the lipid. In one case (replicate 2) we see an exchange of chlorides where one penetrates the membrane, interacts closely with mguanH$^+$, and then is replaced with a second chloride (brown profile) that moves down into the membrane center (labeled Cl^- 1 and Cl^- 2 in Figure 7). The positions of the phosphate groups indicate that the membrane begins to

dx.doi.org/10.1021/jp400389z | J. Phys. Chem. B 2013, 117, 3578−3592

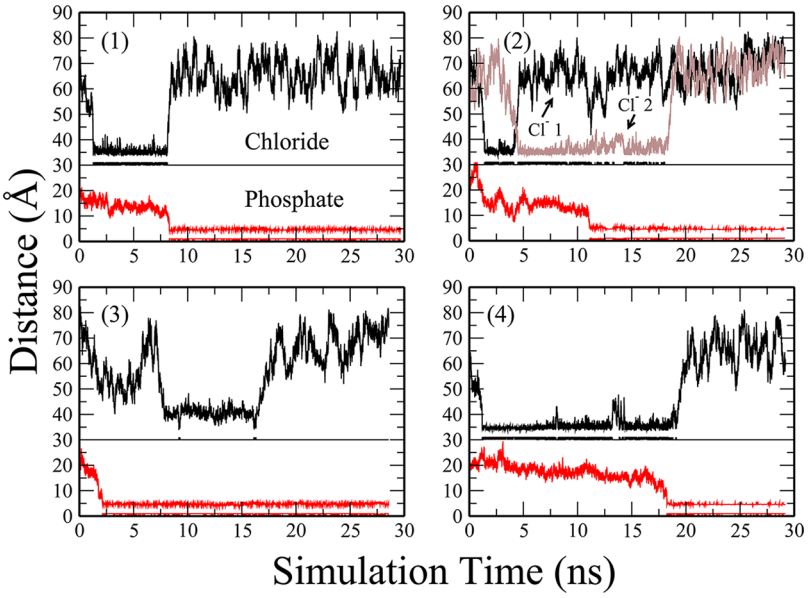

Figure 7. Distance profiles of chloride and lipid phosphate atoms closest to methyl guanidinium for four replicate systems in which mguanH$^+$ is at the center of an initially unperturbed bilayer in which the water constraint has been removed at the beginning of the simulation (time = 0 ns). Profiles are measured as the distance from the mguanH$^+$ center of mass to the chloride and phosphorus atoms. Histograms of the number of associating species are shown below the graphs to indicate when a chloride (black) or lipid phosphorus (red) atom is within 5 Å of the mguanH$^+$ center of mass. Chloride distance profiles and histograms have been offset by 30 Å for clarity. Replicate (2) shows two chloride atoms (the second of which is shown in brown) which are able to move toward the center of the bilayer and associate with mguanH$^+$ at different times during the simulation.

deform from a starting separation of 20 Å from the center mass of the mguanH$^+$ at the beginning of the simulation (consistent with the average position of the unperturbed lipid phosphate headgroups in Figure 6) and slowly moves toward the center of the membrane where it competes with chloride to interact directly with mguanH$^+$. In replicate 3, however, we see the membrane deform quickly, and the phosphate groups are able to associate with mguanH$^+$ before any chlorides can enter the center of the membrane. In the cases where chloride penetrates into the membrane, it does so quickly, on the order of 1 ns or less. Moreover, the chloride is solvated by varying water molecules as it permeates from the bulk and through the membrane, as opposed to moving with a larger, constant solvation structure. Analyzing a sampling of the water that surrounds the chloride atoms in the first hydration shell (within 3.8 Å), we find that, although the chloride stays continuously hydrated throughout the simulation, the water molecules that comprise the hydration shell vary rapidly and are relatively transient. The results of this exercise demonstrate the importance of water in mediating the deformation of phosphate groups, even when the methyl guanidinium is already at the center of the bilayer. This seems to suggest that the deformation of the lipid in terms of one or two phosphate groups associating with the charged species in the bilayer center is the inherent state when the arginine resides in the center. That is, the deformation of the lipid headgroups is not an artifact of the simulation protocol that involves "pulling" along lipid molecules by their headgroups as the methyl guanidinium is slowly (reversibly) transferred into the bilayer via some biasing potential.

IV. SUMMARY AND CONCLUSIONS

We investigated the thermodynamics of permeation of an amino acid side-chain analogue, methyl guanidinium, through a model lipid bilayer, DPPC. Using both umbrella sampling and reweighting in conjunction with average force decomposition, we obtained the potential of mean force for the reversible transfer of methyl guanidinium through the bilayer. We further decomposed the overall PMF into contributions from various system components including water, lipid, ions, and "core" water and lipids. We explored the effects of high salt concentrations in the bulk solution, particularly with respect to the influence of ions on the water contribution to the total PMF. We also investigated the impact of water permeation into the bilayer on lipid deformability. Finally, we performed our calculations using a charge equilibration force field developed in our laboratory (and recently modified as discussed in the Supporting Information of this paper). This is a further application of a new class of force fields that can allow for differences in charge distributions, in a very gross sense, when particular molecular species encounter widely varying electrochemical environments.

With respect to the overall free energetics of methyl guanidinium permeation through the bilayer, our results are qualitatively in agreement with a range of previous simulation studies. We find a free energy minimum in the headgroup region, which is corroborated by molecular dynamics simulations of the unrestrained methyl guanidinium (as shown in Figure S3 of the Supporting Information). We find the potential of mean force for permeation to be approximately 28 kcal/mol (relative to the minimum in the headgroups), within the range of values reported for similar types of simulations using fixed-charge force fields. By decomposing the overall free energy profile into contributions from various components, we find that the lipid in total confers a stabilization of the charge cation in a range from −12 to −100 kcal/mol depending on the ionic strength of the bulk solution. For systems with 1 M KCl salt concentration in the

dx.doi.org/10.1021/jp400389z | J. Phys. Chem. B 2013, 117, 3578−3592

bulk solution, the chloride anion is the sole species destabilizing methyl guanidinium in the bilayer center, with the potassium, water, and lipids all contributing stabilizing forces. In the absence of bulk electrolyte (except for a single chloride anion included in the simulation to maintain charge neutrality), we find that the overall water contribution becomes destabilizing, in stark contrast to the contributions when 1 M KCl is included in the bulk solution. Upon examining differences in local water density and density-weighted forces acting on the permeating cation, we find that the interplay between these two components leads to differences in the asymmetry of water forces on the cation that manifests in two starkly different behaviors. The presence of chloride anions in one case gives rise to an enhancement of local water density as the methyl guanidinium enters the bilayer. These results reinforce current views on the importance of surface active ions of the Hofmeister series and their interactions with phosphatidylcholine-based lipid bilayers, particularly with the penetration of such ions along with hydration layers into the solution−bilayer interface.[56] This enhanced water density in regions around the methyl guanidinium conferring stabilizing forces, relative to the case where no ions are included in the simulation, leads to the observed opposite slope in the water contribution to the total PMF as the methyl guanidinium enters the bilayer. The nature of water contributions to the free energetics of the permeant are similar to the case where no salt is included in the bath in regions along the reaction coordinate where no chloride ions are present. At the core of the bilayer, both systems display stabilizing water contributions arising from a marked water distribution asymmetry.

Finally, we find that water permeation into the bilayer is required for the deformation of individual lipid molecules and permeation of ions into the membrane. Through a series of simulations in which water is first prevented from entering the bilayer center where methyl guanidinium is restrained and after equilibration allowed to enter the bilayer, we find that in the absence of any water defects/permeation into the bilayer the lipid headgroups do not follow the methyl guanidinium. Only after water is allowed to enter the bilayer do we see deformation of individual lipid molecules allowing association with the amino acid analogue at the bilayer center. Moreover, using the force field we have, we find that it is possible for chloride anions to enter the bilayer center very quickly after the water is allowed to enter, thus associating with the methyl guanidinium initially. However, due to the relative energetics of the interaction models used in this work, we observe that the anions in time are displaced by the lipid headgroup phosphates that deform (with the aid of water defects) to associate with the methyl guanidinium. We believe that this suggests that the deformation of the lipid in terms of one or two phosphate groups associating with the charged species in the bilayer center is the inherent state when the arginine resides in the center. Bekker et al.[27] have elegantly demonstrated that the cation, in deforming the membrane, effectively creates an interface that precludes it from experiencing the full positive dipole potential expected for an unperturbed bilayer.[3] The deformation maintains an interface between high and low potential environments, implying that entry of a second charged species would be facilitated by the entry of the first. This nonadditivity has also been demonstrated by MacCallum et al.[26] Thus, the deformation of the lipid headgroups is not an artifact of the simulation protocol that involves "pulling" along lipid molecules by their headgroups as the methyl guanidinium is slowly (reversibly) transferred into the bilayer via some biasing potential. This further supports numerous earlier studies pointing to the importance of water defects on a local scale in facilitating structural and dynamic aspects of membrane biophysics.[12,13,27]

■ ASSOCIATED CONTENT

Supporting Information

Aspects of simulation protocol, refined parameters for the lipid force field and recent modifications, assessment of the convergence of the potentials of mean force, description of uncertainty analysis, further information of position-dependent forces and densities for the various systems discussed in the main text, detailed analysis of effects of water restraint force constants, and details of the core water and lipid decomposition analysis. This material is available free of charge via the Internet at http://pubs.acs.org.

■ AUTHOR INFORMATION

Corresponding Author

*E-mail: sapatel@udel.edu.

Notes

The authors declare no competing financial interest.

■ ACKNOWLEDGMENTS

The authors acknowledge support from the National Science Foundation (CAREER:MCB:1149802). Computational resources are acknowledged via support from National Institutes of Health (COBRE:P20-RR015588) in the Chemical Engineering Department at the University of Delaware. S.P. thanks N. Patel for fruitful discussion and encouragement for the duration of this work.

■ REFERENCES

(1) Dorairaj, S.; Allen, T. W. On the Thermodynamic Stability of a Charged Arginine Sidechan in a Transmembrane Helix. *Proc. Natl. Acad. Sci. U.S.A.* **2007**, *104*, 4943−4948.

(2) Li, L.; Vorobyov, I.; Allen, T. W. Potential of Mean Force and pK_a Profile Calculation for the Lipid Membrane-Exposed Arginine Side Chain. *J. Phys. Chem. B* **2008**, *112*, 9574−9587.

(3) Vorobyov, I.; Li, L.; Allen, T. W. Assessing Atomistic and Coarse-Grained Force Fields for Protein-Lipid Interactions: The Formidable Challenge of an Ionizable Side Chain in a Membrane. *J. Phys. Chem. B* **2008**, *112*, 9588−9602.

(4) Li, L.; Vorobyov, I.; Dorairaj, S.; Allen, T. W. Charged Protein Side Chain Movement in Lipid Bilayers Explored with Free Energy Simulation. *Curr. Top. Membr.* **2008**, *60*, 505−459.

(5) Schow, E. V.; Freites, J. A.; Cheng, P.; Bernsel, A.; von Heijne, G.; White, S. H.; Tobias, D. J. Arginine in Membranes: The Connection Between Molecular Dynamics Simulations and Translocon-mediated Insertion Experiments. *J. Membr. Biol.* **2011**, *239*, 35−48.

(6) Gumbart, J.; Roux, B. Determination of Membrane-Insertion Free Energies by Molecular Dynamics Simulations. *Biophys. J.* **2012**, *102*, 795−801.

(7) Fleming, P. J.; Freites, J. A.; Moon, C. P.; Tobias, D. J.; Fleming, K. G. Outer Membrane Phospholipase A in Phospholipid Bilayers: A Model System for Concerted Computational and Experimental Investigations of Amino Acid Side Chain Partitioning Into Lipid Bilayers. *Biochim. Biophys. Acta, Biomembr.* **2012**, *1818*, 126−134.

(8) Moon, C. P.; Fleming, K. G. Side-chain hydrophobicity scale derived from transmembrane protein folding into lipid bilayers. *Proc. Natl. Acad. Sci. U.S.A.* **2011**, *108*, 10174−10177.

(9) Yoo, J.; Cui, Q. Does Arginine Remain Protonated in the Lipid Membrane? Insights from Microscopic pKa Calculations. *Biophys. J.* **2008**, *94*, L61−L63.

(10) Hristova, K.; Wimley, W. C. A Look at Arginine in Membranes. *J. Membr. Biol.* **2011**, *239*, 253−259.
(11) Tieleman, D. P.; MacCallum, J. L.; Ash, W. L.; Kandt, C.; Xu, Z.; Monticelli, L. M. Membrane Protein Simulations with a United Atom Lipid and All Atom Protein Model: Side Chain Transfer Free Energies and Model Proteins. *J. Phys.: Condens. Matter* **2006**, *18*, S1221−S1234.
(12) MacCallum, J. L.; Bennett, W. F. D.; Tieleman, D. P. Distribution of Amino Acids in a Lipid Bilayer from Computer Simulations. *Biophys. J.* **2008**, *94*, 3393−3404.
(13) MacCallum, J. L.; Bennett, W. F. D.; Tieleman, D. P. Partitioning of Amino Acid Side Chains into Lipid Bilayers: Results from Computer Simulations and Comparison to Experiment. *J. Gen. Physiol.* **2007**, *129*, 371−377.
(14) Jiang, Y.; Lee, A.; Chen, J.; Ruta, V.; Cadene, M.; Chait, B. T.; MacKinnon, R. X-ray Structure of a Voltage-Dependent K+ Channel. *Nature* **2003**, *423*, 33−41.
(15) Jiang, Y.; Lee, A.; Chen, J.; Cadene, M.; Chait, B. T.; MacKinnon, R. The Open Pore Conformation of Potassium Channels. *Nature* **2002**, *417*, 523−526.
(16) Jensen, M. O.; Jogini, V.; Borhani, D. W.; Leffler, A. E.; Dror, R. O.; Shaw, D. E. Mechanism of Voltage Gating in Potassium Channels. *Science* **2012**, *336*, 229−233.
(17) Herce, H. D.; Garcia, A. E. Cell Penetrating Peptides: How Do They Do It? *J. Biol. Phys.* **2007**, *33*, 345−356.
(18) Marks, J.; Placone, J.; Hristova, K.; Wimley, W. C. Spontaneous Membrane-Translocating Peptides by Orthogonal High-Throughput Screening. *J. Am. Chem. Soc.* **2011**, *133*, 8995−9004.
(19) Herce, H. D.; Garcia, A. E.; Litt, J.; Kane, R. S.; Martin, P.; Enrique, N.; Rebolledo, A.; Milesi, V. Arginine-Rich Peptides Destabilize the Plasma Membrane, Consistent with a Pore Formation Translocation Mechanism of Cell-Penetrating Peptides. *Biohys. J.* **2009**, *97*, 1917−1925.
(20) Jarver, P.; Langel, U. Cell-Penetrating Peptides: A Brief Introduction. *Biochim. Biophys. Acta, Biomembr.* **2006**, *1758*, 260−263.
(21) Vives, E.; Schmidt, J.; Pelegrin, A. Cell-Penetrating and Cell-Targeting Peptides in Drug Delivery. *Biochim. Biophys. Acta, Revi. Cancer* **2008**, *1786*, 126−138.
(22) Futaki, S. Oligorarginine Vectors for Intracelular Delivery: Design and Cellular - Uptake Mechanisms. *Biopolymers* **2006**, *84*, 241−249.
(23) Lattig-Tunnemann, G.; Prinz, M.; Hoffmann, D.; Behlke, J.; Palm-Apergi, C.; Morano, I.; Herce, H. D.; Cardoso, M. C. Backbone Rigidity and Static Presentation of Guanidinium Groups Increases Cellular Uptake of Arginine-Rich Cell-Penetrating Peptides. *Nat. Commun.* **2011**, *2*, 453−458.
(24) MacCallum, J. L.; Tieleman, D. P. Hydrophobicity Scales: A Thermodynamic Looking Glass Into Lipid-Protein Interactions. *Trends Biochem. Sci.* **2011**, *36*, 653−662.
(25) Hessa, T.; White, S. H.; von Heijne, G. Membrane Insertion of a Potassium Channel Voltage Sensor. *Science* **2005**, *307*, 1427−1427.
(26) MacCallum, J. L.; Bennett, W. F. D.; Tieleman, D. P. Transfer of Arginine Into Lipid Bilayers is Nonadditive. *Biophys. J.* **2011**, *101*, 110−117.
(27) Vorobyov, I.; Bekker, B.; Allen, T. W. Electrostatics of Deformable Lipid Membranes. *Biophys. J.* **2010**, *98*, 2904−2913.
(28) Bogdanov, M.; Xie, J.; Dowhan, W. Lipid−Protein Interactions Drive Membrane Protein Topogenesis in Accordance with the Positive Inside Rule. *J. Biol. Chem.* **2009**, *284*, 9637−9641.
(29) Bogdanov, M.; Heacock, P. N.; Dowhan, W. A Polytopic Membrane Protein Displays a Reversible Topology Dependent on Membrane Lipid Composition. *EMBO J.* **2002**, *21*, 2107−2116.
(30) Bogdanov, M.; Xie, J.; Heacock, P. N.; Dowhan, W. To Flip or Not to Flip: Lipid-Protein Charge Interactions are a Determinant of the Final Membrane Protein Topology. *J. Cell Biol.* **2008**, *182*, 925−935.
(31) Zhang, W.; Bogdanov, M.; Pi, J.; Pittard, A. J.; Dowhan, W. Reversible Topological Organization Within a Polytopic Membrane Protein is Governed by a Change in Membrane Phospholipid Composition. *J. Biol. Chem.* **2003**, *278*, 50128−50135.
(32) Wimley, W. C.; Hristova, K. Antimicrobial Peptides: Successes, Challenges, and Unanswered Questions. J. Membr. Biol. *J. Membr. Biol.* **2011**, *239*, 27−34.
(33) Gresh, N.; Cisneros, G. A.; Darden, T. A.; Piquemal, J.-P. Anisotropic, Polarizable Molecular Mechanics Studies of Inter- and Intramolecular Interactions and Ligand-Macromolecule Complexes. A bottom-up Strategy. *J. Chem. Theory Comput.* **2007**, *3*, 1960−1986.
(34) Piquemal, J.-P.; Perera, L.; Cisneros, G. A.; Ren, P.; Pedersen, L. G.; Darden, T. A. Towards Accurate Solvation Dynamics of Divalent Cations in Water Using the Polarizable Amoeba Force Field: From Energetics to Structure. *J. Chem. Phys.* **2006**, *125* (054511), 1−7.
(35) de Courcy, B.; Piquemal, J.-P.; Garbay, C.; Gresh, N. Polarizable Water Molecules in Ligand-Macromolecule Recognition. Impact on the Relative Affinities of Competing Pyrrolopyrimidine Inhibitors for FAK Kinase. *J. Am. Chem. Soc.* **2010**, *132*, 3312−3320.
(36) Jiao, D.; King, C.; Grossfield, A.; Darden, T. A.; Ren, P. Simulation of Ca^{2+} and Mg^{2+} Solvation Using Polarizable Atomic Multipole Potential. *J. Phys. Chem. B* **2006**, *110*, 18553−18559.
(37) Ponder, J. W.; Wu, C.; Ren, P.; Pande, V. S.; Chodera, J. D.; Schnieders, M. J.; Haque, I.; Mobley, D. L.; Lambrecht, D. S.; DiStasio, R. A., Jr.; Head-Gordon, M.; Clark, G. N. I.; Johnson, M. E.; Head-Gordon, T. Current Status of the AMOEBA Polarizable Force Field. *J. Phys. Chem. B* **2010**, *114*, 2549−2564.
(38) Jiao, D.; Golubkov, P. A.; Darden, T. A.; Ren, P. Calculation of Protein-Ligand Binding Free Energy by Using a Polarizable Potential. *Proc. Natl. Acad. Sci.* **2008**, *105*, 6290−6295.
(39) Anisimov, V. M.; Lamoureux, G.; Vorobyov, I. V.; Huang, N.; Roux, B.; MacKerell, A. D., Jr. Determination of Electrostatic Parameters for a Polarizable Force Field Based on the Classical Drude Oscillator. *J. Chem. Theory Comput.* **2005**, *1*, 153−168.
(40) Lamoureux, G.; Roux, B. Modeling Induced Polarization with Classical Drude Oscillators: Theory and Molecular Dynamics Simulations Algorithm. *J. Chem. Phys.* **2003**, *119* (3025), 1−15.
(41) Lamoureux, G.; MacKerell, A. D., Jr.; Roux, B. A Simple Polarizable Model of Water Based on Classical Drude Oscillators. *J. Chem. Phys.* **2003**, *119* (5185), 1−13.
(42) Lamoureux, G.; Harder, E.; Vorobyov, I. V.; Roux, B.; MacKerell, A. D., Jr. Polarizable Model of Water for Molecular Dynamics Simulations of Biomolecules. *Chem. Phys. Lett.* **2006**, *418*, 245−249.
(43) Lopes, P. E. M.; Lamoureux, G.; Roux, B.; MacKerell, A. D., Jr. Polarizable Empirical Force Field for Aromatic Compounds Based on the Classical Drude Oscillator. *J. Phys. Chem. B* **2007**, *111*, 2873−2885.
(44) Yu, H.; Whitfield, T. W.; Harder, E.; Lamoureux, G.; Vorobyov, I.; Anisimov, V. M.; MacKerell, A. D., Jr.; Roux, B. Simulating Monovalent and Divalent Ions in Aqueous Solution Using a Drude Polarizable Force Field. *J. Chem. Theory Comput.* **2010**, *6*, 774−786.
(45) Harder, E.; MacKerell, A. D., Jr.; Roux, B. Many-Body Polarization Effects and the Membrane Dipole Potential. *J. Am. Chem. Soc.* **2009**, *131*, 2760−2761.
(46) Patel, S.; MacKerell, A. D., Jr.; Brooks, C. L., III CHARMM Fluctuating Charge Force Fields for Proteins: II. Protein/Solvent Properties from Molecular Dynamics Simulations Using a Nonadditive Electrostatic Model. *J. Comput. Chem.* **2004**, *25*, 1504−1514.
(47) Patel, S.; Brooks, C. L., III A Nonadditive Methanol Force Field: Bulk Liquid and Liquid-Vapor Interfacial Properties via Molecular Dynamics Simulations Using a Fluctuating Charge Model. *J. Chem. Phys.* **2005**, *122* (024508), 1−10.
(48) Patel, S.; Brooks, C. L., III Structure, Thermodynamics, and Liquid-Vapor Equilibrium of Ethanol from Molecular Dynamics Simulations Using Nonadditive Interactions. *J. Chem. Phys.* **2005**, *123* (164502), 1−12.
(49) Bauer, B. A.; Lucas, T. R.; Meninger, D.; Patel, S. Water Permeation Through DMPC Lipid Bilayers Using Polarizable Charge Equilibration Force Fields. *Chem. Phys. Lett.* **2011**, *508*, 289−294.
(50) Lucas, T. R.; Bauer, B. A.; Davis, J. E.; Patel, S. Molecular Dynamics Simulation of Hydrated DPPC Monolayers Using Charge Equilibration Force Fields. *J. Comput. Chem.* **2012**, *33*, 141−152.

(51) Davis, J. E.; Patel, S. Revised Charge Equilibration Parameters for More Accurate Hydration Free Energies of Alkanes. *Chem. Phys. Lett.* **2010**, *484*, 173−176.
(52) Zhong, Y.; Patel, S. Nonadditive Empirical Force Fields for Short-Chain Linear Alcohols: Methanol to Butanol. Hydration Free Energies and Kirkwood-Buff Analysis Using Charge Equilibration Models. *J. Phys. Chem. B* **2010**, *114*, 11076−11092.
(53) Warren, G. L.; Davis, J. E.; Patel, S. Origin and Control of Superlinear Polarizability Scaling in Chemical Potential Equilization Methods. *J. Chem. Phys.* **2008**, *128* (144110), 1−14.
(54) Davis, J. E.; Rahaman, O.; Patel, S. Molecular Dynamics Simulations of a DMPC Bilayer Using Nonadditive Interaction Models. *Biophys. J.* **2009**, *96*, 385−402.
(55) Shimizu, K.; Chaimovich, H.; Farah, J. P. S.; Dias, L. G.; Bostick, D. L. Calculation of the Dipole Moment for Polypeptides Using the Generalized Born-Electronegativity Equalization Method: Results in Vacuum and Continuum-Dielectric Solvent. *J. Phys. Chem. B* **2004**, *108*, 4171−4177.
(56) Vacha, R.; Jurkiewicz, P.; Petrov, M.; Berkowitz, M. L.; Bockmann, R. A.; Barucha-Kraszewska, J.; Hof, M.; Jungwirth, P. Mechanism of Interaction of Monovalent Ions with Phosphatidylcholine Lipid Membranes. *J. Phys. Chem. B* **2010**, *114*, 9504−9509.
(57) Davis, J. E.; Patel, S. Charge Equilibration Force Fields for Lipid Environments: Applications to Fully Hydrated DPPC Bilayers and DMPC-Embedded Gramicidin A. *J. Phys. Chem. B* **2009**, *113*, 9183−9196.
(58) Patel, S.; Brooks, C. L., III CHARMM Fluctuating Charge Force Fields for Proteins: I Parameterization and Application to Bulk Organic Liquid Simulations. *J. Comput. Chem.* **2004**, *25*, 1−15.
(59) Patel, S.; Brooks, C. L., III Fluctuating Charge Force Fields: Recent Developments and Applications from Small Molecules to Macromolecular Biological Systems. *Mol. Simul.* **2006**, *32*, 231−249.
(60) Rappe, A. K.; Goddard, W. A. Charge Equilibration for Molecular Dynamics Simulations. *J. Phys. Chem.* **1991**, *95*, 3358−3363.
(61) Rick, S. W.; Stuart, S. J.; Berne, B. J. Dynamical Fluctuating Charge Force Fields: Application to Liquid Water. *J. Chem. Phys.* **1994**, *101*, 6141−6156.
(62) Rick, S. W.; Stuart, S. J.; Bader, J. S.; Berne, B. J. Fluctuating Charge Force Fields for Aqueous Solutions. *J. Mol. Liq.* **1995**, *65/66*, 31−40.
(63) Rick, S. W.; Berne, B. J. Dynamical Fluctuating Charge Force Fields: The Aqueous Solvation of Amides. *J. Am. Chem. Soc.* **1996**, *118*, 672−679.
(64) Rick, S. W. Simulations of Ice and Liquid Water Over a Range of Temperatures Using the Fluctuating Charge Model. *J. Chem. Phys.* **2001**, *114*, 2276−2283.
(65) Rick, S. W.; Stuart, S. J. *Reviews of Computational Chemistry*; John Wiley & Sons: New York, 2002; pp 89−146.
(66) Sanderson, R. T. An Interpretation of Bond Lengths and a Classification of Bonds. *Science* **1951**, *114*, 670−672.
(67) Sanderson, R. T. *Chemical Bonds and Bond Energy*; Academic Press: New York, 1976.
(68) Nalewajski, R. F.; Korchowiec, J.; Zhou, Z. Molecular Hardness and Softness Parameters and Their Use in Chemistry. *Int. J. Quantum Chem.* **1988**, *22*, 349−366.
(69) Lee, A. J.; Rick, S. W. The Effects of Charge Transfer on the Properties of Liquid Water. *J. Chem. Phys.* **2011**, *134* (184507), 1−9.
(70) Chelli, R.; Procacci, P.; Righini, R.; Califano, S. Electrical Response in Chemical Potential Equalization Schemes. *J. Chem. Phys.* **1999**, *111*, 8569−8575.
(71) Davis, J. E.; Warren, G. L.; Patel, S. Revised Charge Equilibration Potential for Liquid Alkanes. *J. Phys. Chem. B* **2008**, *112*, 8298−8310.
(72) Ren, P.; Ponder, J. W. Polarizable Atomic Multipole Water Model for Molecular Mechanics Simulation. *J. Phys. Chem. B* **2003**, *107*, 5933−5947.
(73) Car, R.; Parrinello, M. Unified Approach for Molecular Dynamics and Density Functional Theory. *Phys. Rev. Lett.* **1985**, *55*, 2471−2474.
(74) Biltonen, R. L.; Lichtenberg, D. The Use of Differential Scanning Calorimetry as a Tool to Characterize Liposome Preparations. *Chem. Phys. Lipid* **1993**, *64*, 129−142.
(75) Kučerka, N.; Nagle, J. F.; Sachs, J. N.; Feller, S. E.; Pencer, J.; Jackson, A.; Katsaras, J. Lipid Bilayer Structure Determined by the Simultaneous Analysis of Neutron and X-ray Scattering Data. *Biophys. J.* **2008**, *95*, 2356−2367.
(76) Allen, M. P.; Tildesley, D. J. *Computer Simulations of Liquids*; Clarendon: U.K., 1987.
(77) Nosé, S. A Molecular Dynamics Methods for Simulations in the Canonical Ensemble. *Mol. Phys.* **1984**, *52*, 255−268.
(78) Darden, T.; York, D.; Pedersen, L. Particle Mesh Ewald: An $N \cdot \log(N)$ Method for Ewald Sums in Large Systems. *J. Chem. Phys.* **1993**, *98*, 10089−10092.
(79) Essmann, U.; Darden, T.; Lee, H.; Perera, L.; Berkowitz, M. L.; Pederson, L. A Smooth Particle Mesh Ewald Method. *J. Chem. Phys.* **1995**, *103*, 8577−8593.
(80) Patel, S.; Davis, J. E.; Bauer, B. A. Exploring Ion Permeation Energetics in Gramicidin A Using Polarizable Charge Equilibration Force Fields. *J. Am. Chem. Soc.* **2009**, *131*, 13890−13891.
(81) Zhong, Y.; Bauer, B. A.; Patel, S. Solvation Properties of *N*-Acetyl-β-glucosamine: A Molecular Dynamics Study Incorporating Electrostatic Polarization. *J. Comput. Chem.* **2011**, *32*, 3339−3353.
(82) Li, L. B.; Vorobyov, I.; Allen, T. W. The Role of Membrane Thickness in Charged Protein-Lipid Interactions. *Biochim. Biophys. Acta, Biomembr.* **2012**, *1818*, 135−145.
(83) Warren, G. L.; Patel, S. Hydration Free Energies of Monovalent Ions in Transferable Intermolecular Potential Four Point Fluctuating Charge Water: An Assessment of Simulation Methodology and Force Field Performance and Transferability. *J. Chem. Phys.* **2007**, *127* (064509), 1−19.
(84) Lynden-Bell, R. M.; Rasaiah, J. C. From Hydrophobic to Hydrophillic Behaviour: A Simulation Study of Solvation Entropy and Free Energy of Simple Solutes. *J. Chem. Phys.* **1997**, *107*, 1981−1991.
(85) Shirts, M. R.; Pande, V. S. Solvation Free Energies of Amino Acid Side Chain Analogs for Common Molecular Mechanics Water Models. *J. Chem. Phys.* **2005**, *122* (134508), 1−13.
(86) Harder, E.; Roux, B. On the Origin of the Electrostatic Potential Difference at a Liquid-Vacuum Interface. *J. Chem. Phys.* **2008**, *129* (234706), 1−9.
(87) Kumar, S.; Bouzida, D.; Swendsen, R. H.; Kollman, P. A.; Rosenberg, J. M. The Weighted Histogram Analysis Method for Free-Energy Calculations on Biomolecules. I. The Method. *J. Comput. Chem.* **1992**, *13*, 1011−1021.
(88) Beglov, D.; Roux, B. Finite Representation of an Infinite Bulk System: Solvent Boundary Potential for Computer Simulations. *J. Chem. Phys.* **1994**, *100* (9050), 1−14.
(89) Zhu, F.; Hummer, G. Convergence and Error Estimation in Free Energy Calculations Using the Weighted Histogram Analysis Method. *J. Comput. Chem.* **2011**, *33*, 453−465.
(90) Flyvbjerg, H.; Petersen, H. G. Error Estimates on Averages of Correlated Data. *J. Chem. Phys.* **1989**, *91*, 461−466.
(91) Patel, S.; Brooks, C. L., III Revisiting the Hexane-Water Interface via Molecular Dynamics Simulations Using Nonadditive Alkane-Water Potentials. *J. Chem. Phys.* **2006**, *124* (204706), 1−14.
(92) Vorobyov, I. V.; Anisimov, V. M.; A. D. MacKerell, J. Polarizable Empirical Force Field for Alkanes Based on the Classical Drude Oscillator Model. *J. Phys. Chem. B* **2005**, *109*, 18988−18999.
(93) Frisch, M. J. et al. *Gaussian 03*, revision D.02; Gaussian, Inc.: Wallingford, CT, 2004.